Multiscale Study of Counterion-Induced Attraction and Bundle Formation of F-Actin Using an Ising-like Mean-Field Model

Xueping Yu and A. E. Carlsson
Physics Department, Washington University, St. Louis, Missouri

ABSTRACT An Ising-like counterion-binding model is developed and solved by a mean-field method. For G-actin, the calculated affinity constants of all the binding sites ranging from loose to tight binding match the experimental data. The model is used to calculate the interaction energy between two F-actin filaments. Within a certain counterion concentration range, a rapidly decaying attractive force between two parallel filaments is produced not only by the correlation of the counterion distributions on the two filaments, but also by the correlation of the configurations of the two filaments with fixed counterion positions, which has been ignored in previous calculations. The bundling energy depends strongly on the configuration of the filaments. Upon bundling, the tightly bound counterion site is not affected, but the medium and loosely bound ones are. The model reproduces the observed minimal divalent counterion concentration for bundling, and naturally predicts the resolubilization of bundles which is seen in recent experiments. At the optimal counterion concentration, we obtain a bundling energy of ~ -0.01 eV per monomer along the filament. The counterion valence strongly affects the optimal counterion concentration, but has only minor effects on the optimal bundling energy. We show that the attractive potential between filaments can be simplified as the sum of interactions between their monomers. This simplification makes it possible to calculate the exact free energy of a two-F-actin-filament system. We are thus able to probe the effects of filament length on F-actin bundling and obtain a critical length for bundling of 59 monomers at 1 μM monomer concentration and pH $= 7.2$.

INTRODUCTION

Two polyelectrolytes with the same charge would naturally be expected to repel each other (Grønbech-Jensen et al., 1997). But in sufficiently high concentrations of polyvalent counterions, DNA (Bloomfield, 1996, 1997), F-actin filaments (Kawamura and Maruyama, 1970; Tang and Janmey, 1996; Tang et al., 1996), microtubules (Tang et al., 1996), and other like-charged entities can condense or bundle together. Even single DNA molecules can form toroids (Baeza et al., 1987), and F-actin can form rings (Tang et al., 2001) in the presence of polyvalent salt. These observations show that polyvalent counterions can mediate a lateral attraction between two like-charged polyelectrolytes or two parts of one polyelectrolyte. This has also been confirmed by simulation results for rods (Grønbech-Jensen et al., 1997; Stevens, 2001, 1999) and plates (Moreira and Netz, 2001; Lau and Pincus, 2002). This counterintuitive attraction between like-charged objects cannot be explained by the mean-field approaches of Debye-Hückel or Poisson-Boltzmann theory unless some correlations or other corrections are introduced. Two approaches have been used to explain the counterion-mediated attractions (Gelbart et al., 2000) in the correlation picture. The first involves a fluctuation correction to the Poisson-Boltzmann mean-field theory. The attractive term is analogous to the van der Waals force except that it is mediated by classical mobile counterions instead of quantum mechanical electrons. Correlated thermal fluctuations of the condensed counterion density along two rodlike macroions has been studied (Oosawa, 1968) in this approach using the dipole approximation. The attractive force for two rods of high Manning parameter ($\lambda Q/\varepsilon kT$, where λ is the line charge density of the rod and Q is the charge of counterions) was found to be proportional to T/R^2, where T is temperature and R is the distance between the two rods. This dipole correction is inadequate when R is much shorter than the length of the rods. The second approach does not begin with mean-field theory. Instead it treats the counterions explicitly to some extent by simplified models or simulations (Ha and Liu, 1997; Stevens, 1999; Grønbech-Jensen et al., 1997; Diehl et al., 2001; Deserno and Holm, 2002) and includes multipole interactions and correlations naturally. It focuses on the short-range electrostatic correlations of the counterions on the two polyelectrolytes. Unlike the previous mechanism, low temperature enhances the attractive force (Grønbech-Jensen et al., 1997). Ray and Manning also suggested a theory, which focuses on the interface between the condensed and diffuse counterion layers, to explain the counterion-induced attractive forces (Ray and Manning, 1994; Manning, 2003).

F-actin bundling or DNA condensation is determined by the competition between the attractive force, which favors bundling or condensation, and the entropy, which opposes it. The attractive force is induced by appropriate concentrations of counterions with high valence and strong binding affinity to the polyelectrolyte. Increasing the filament length can also enhance the attractive force. These factors have been clarified in a systematic series of bundling experiments (Tang and Janmey, 1996). The entropic contribution can be reduced by increasing the stiffness of the polyelectrolyte. Although linear DNA requires counterions of valence at least

Submitted June 3, 2003, and accepted for publication August 6, 2003.

Address reprint requests to Xueping Yu, Campus Box 1105, Washington University, Dept. of Physics, One Brookings Drive, St. Louis, MO 63130. Tel.: 314-935-5739; Fax: 314-935-6219; E-mail: xyu@artsci.wust1.edu.

0006-3495/03/12/3532/12 $2.00

3 to aggregate (Bloomfield, 1996), supercoiled DNA, which is stiffer and thus has less conformational entropy, can condense under physiological concentrations of divalent counterions (Ma and Bloomfield, 1994; Bednar et al., 1994). A few experiments (Bruno and Mattice, 1992; Sedlak and Amis, 1992; Borsali et al., 1998; Manning, 2003) have shown that even monovalent counterions can cause DNA or other polyelectrolyte molecules to condense at dilute polyelectrolyte concentrations. A simple bead-spring chain model has been used (Stevens, 1999) to study the factors of filament length, stiffness, and counterion valence via molecular dynamics simulations. This model showed that sufficiently long and rigid filaments and divalent counterions are necessary for the filaments to form oriented bundles. Unlike other theoretical approaches, the calculations of Borukhov et al. (2002) treated the aggregation of semiflexible filaments using the effective interaction between the linkers (aggregation agents) instead of the interaction between the filaments, and showed that the filament rigidity is the dominant factor in this effective interaction. To our knowledge, the most complete calculations of bundling for mesoscopic systems have been performed for DNA (Kornyshev and Leikin, 1998). They obtained bundling interactions by fixing the counterion positions and simplifying the DNA structure somewhat.

In this article, we present results for F-actin bundling performed using a realistic atomic structure, and study the dependence of bundling on the counterion concentration. Our simplified model, mean-field approach, and largest-error-correction algorithm, described in the next section, allow us to place counterions accurately in the atomic-level filament structures. Using these atomic structures, we obtain a broad range of results which can be compared to experimental data and cannot be obtained by simpler approaches, including binding patterns (the set of the probabilities for sites in a protein to bind specific counterions), affinity constants, and the dependence of the attractive force on the two filaments' spatial configuration (rotations around their center lines and relative displacement). We also vary the counterion concentrations in our model so that we can study the dependence of the attractive potential on counterion concentration.

There are two important approximations in our microscopic model. The first is that only electrostatic interactions and a simplified form of steric interactions are considered. As the second and the most important approximation, water is treated as a uniform dielectric medium, and the counterion solution is modeled by a background whose functions are to provide counterions to occupy the discrete binding sites (BS) on the polyelectrolyte and to generate long range screening; only the bound counterions are involved in the electrostatic interactions, except for Debye screening effects. The bound nature of the counterions does not mean that they are immobile; they can move around one BS, jump to another BS or escape to the solution. The binding probability (discussed later) of bound counterions to a BS describes the counterion density around this BS. The counterion concentration determines the ability of the background to provide counterions. The explicit treatment of counterions already includes the short-range screening, and we include no additional effects of this type. We model longer-ranged screening with the Debye-Hückel form $\exp[-\kappa(r - r_b)]$ at larger distances ($r > r_b$), where κ is the Debye-Hückel screening constant and r_b is a cutoff distance.

The organization of the remainder of the article is as follows. The next section introduces the counterion binding model, which includes protons as well as divalent counterions (to avoid confusion, we do not use the term *counterion* to refer to protons). In the following section, we apply our Ising-like mean-field model to G-actin and study the hierarchy of binding sites. In following sections, the interaction between two parallel F-actin filaments is evaluated, and a short-ranged attractive interaction is found within a limited range of divalent counterion concentrations. The counterion concentration which neutralizes the F-actins gives the largest attractive force. Extremely high concentrations can overcharge the F-actins, as discussed in Shklovskii (1999). This makes the interaction repulsive or only weakly attractive so that debundling occurs. This debundling phenomenon was recently confirmed (Tang et al., 2002) and denoted *resolubilization*. After obtaining the counterion-mediated attraction between F-actin filaments, we study the statistical mechanics of F-actin bundling. We first simplify the attractive potential to a sum of analytically expressed interaction terms between their monomers. With this simplification, we calculate the exact free energy of the two-F-actin system and discuss the relation of F-actin bundling to filament length and actin concentration.

Counterion binding model

We assume that the counterions interact only with charged amino acids Arg, Lys, and His, which can bind a proton and be positively charged, or Asp and Glu, which can lose a proton and be negatively charged. The counterions concentrate near the negatively charged sites. The protons can also bind to some neutral sites. Our main approximation is that a counterion or proton can have two states: bound at a site, or free. The electrostatic interactions involving the free state are ignored. For simplicity, the bound counterion is regarded as having the position of its binding site in evaluating interactions with other sites and their bound counterions. For a particular type of counterion, a binding site on the protein thus has two states: occupied or unoccupied, like a spin in the Ising model. Therefore in our model we consider only the binding sites, their binding states, and the electrostatic fields from all charges. This approach extends those of Ha and Liu (1997) and Diehl et al. (2001), which treated a periodic array of binding sites on idealized filaments. Our approach uses a more accurate

atomic structure than that used in the DNA-bundling calculations of Kornyshev and Leikin (1998). Unlike their model, our model accounts for rearrangements of bound counterions.

We obtain the atomic structures from the Protein Data Bank (PDB). As in the simpler version of the CHARMM approach using the ''charmm21.chg'' file (Brooks et al., 1983), the charges are assigned as follows: $-0.5\ e$ to $O_{\delta 1}$ and $O_{\delta 2}$ of Asp, $O_{\varepsilon 1}$ $O_{\varepsilon 2}$ of Glu, $O_{1\alpha}$, $O_{2\alpha}$, $O_{1\beta}$, and $O_{2\beta}$ of ATP; $-2/3\ e$ to $O_{1\gamma}$, $O_{2\gamma}$ and $O_{3\gamma}$ of ATP; $0.5\ e$ $N_{\eta 1}$ and $N_{\eta 2}$ of Arg; and $1\ e$ to N_{ζ} of Lys. The N-terminal, if it is not acetylated (for actin the N-terminal is acetylated), and the C-terminal, are also assigned charges. Unlike Arg and Lys, which have pK_d values >10 and always bind protons if the pH value is not too high, the pK_d value of His is 6.04 (Lide, 2000) and its proton binding is very sensitive to pH. The model starts with neutral His and allows it to bind a proton on $N_{\delta 1}$ or $N_{\varepsilon 2}$ to give positive charges whose magnitude is determined by the pH value and polyvalent counterion concentration according to our algorithm described below. All negatively charged atoms are binding sites for both types of counterions.

Like the Ising model, the model can be treated by mean-field methods to reduce the computation relative to other methods, such as Monte Carlo simulation. We found the Monte Carlo approach impractical for calculating filament-filament interactions. However, we have performed Monte Carlo calculations for single monomer counterion binding, and find results similar to the mean-field results. We use the binding probability arrays $\{m_i\}$ and $\{h_i\}$ of counterions and protons, respectively, to sites i, to describe the state of the system. The free energy of the counterion-proton system, G_{MP}, is written as

$$
\begin{aligned}
G_{MP} = {} & \frac{1}{2}\sum_{i\neq j}\frac{q_i q_j D(r_{ij})}{\varepsilon r_{ij}} + \sum_{i\neq j}\frac{q_i m_j Q D(r_{ij})}{\varepsilon r_{ij}} + \frac{1}{2}\sum_{i\neq j}\frac{m_i m_j Q^2 D(r_{ij})}{\varepsilon r_{ij}} + \sum_{i}\frac{(q_i - q_{ref})m_i Q}{\varepsilon r_{sm}} - kT\sum_{i} m_i \ln(c_m/c_0) + kT\sum_{i} m_i \ln m_i \\
& + kT\sum_{i}(1-m_i)\ln(1-m_i) + \sum_{i\neq j}\frac{q_i h_j e D(r_{ij})}{\varepsilon r_{ij}} + \frac{1}{2}\sum_{i\neq j}\frac{h_i h_j e^2 D(r_{ij})}{\varepsilon r_{ij}} + \sum_{q_i>0}\frac{(q_i - q_{ref})h_i e}{\varepsilon r_{sh}} - kT\sum_{i} h_i \ln(c_p/c_{p0}^{i}) \\
& + kT\sum_{i} h_i \ln h_i + kT\sum_{i}(1-h_i)\ln(1-h_i) + \sum_{i\neq j}\frac{m_i h_j Q e D(r_{ij})}{\varepsilon r_{ij}} + \sum_{q_i>0}\frac{m_i h_j Q e}{\varepsilon r_{mh}},
\end{aligned}
\tag{1}
$$

with the restrictions $m_i = 0$ for all $q_i \geq 0$ and $h_\iota = 0$ for all $q_i > 0$. Here, q_i is charge of site i in the absence of counterions, ε is the dielectric constant of water ($\varepsilon = 78$), Q is the counterion charge, r_{ij} is the distance between sites i and j, r_{sm} is the distance of a binding site to its bound counterion, c_m is the concentration of counterions, q_{ref} is a reference charge of $-0.5\ e$, and c_0 is the dissociation constant of an isolated hypothetical binding site of charge q_{ref} with all other charged sites neutralized. We deal with generic divalent counterions and c_0 is assumed to be the same for all sites. We thus ignore their local geometrical and chemical environment differences. Term 1 contains the Coulomb interactions between the charged sites. Terms 2 and 3 in Eq. 1 are Coulomb interactions involving site charges and counterions. Terms 4 and 5 describe the competition between the attachment energy to the binding site and the higher counterion entropy in the free state. Term 4 accounts for the interactions between counterions and the binding sites closest to them. These interactions vary from site to site because of the variations in q_i. Thus the model includes both a localized interaction between a counterion and a particular binding site, and a more delocalized interaction with other charged sites. The localized interactions are too weak to bind counterions, so the delocalized terms are essential. The variations in Term 4 affect the affinity of the tightly bound site only weakly, and the other results are quite insensitive to the value of r_{sm}. We choose $r_{sm} = 2.7$ Å, because it is a typical distance between divalent metal ions and oxygen atoms. We have also tried $r_{sm} = 3.7$ Å, and the only noticeable difference is in the k_d value of the tightly bound site which changes from 23 nM to 27 nM.

In Term 5, the interaction of divalent counterions with a single binding site charged with $-0.5\ e$ is in some ways analogous to the interaction between monovalent ions, for example Na^+ and Cl^-, in a salt solution. At a concentration of 6 M, Na^+, and Cl^- bind and form a crystal. So, as a rough estimate, we take $c_0 = 5$ M. With this choice of c_0, we obtain a high-affinity binding constant matching the experimental one in the next section. Changes in the value of c_0 can shift the concentration-related quantities, such as affinity constants, but do not affect the binding patterns or the value of the attractive interaction at the optimal counterion concentration. Terms 6 and 7 include the entropy associated with the binding probability, which has a maximum when all sites are half occupied. In the analogous uncoupled Ising spin system, the spins have a probability of a 1/2 to be up or down.

Terms 8–13 are analogs, for protons, of terms 2–7. Terms 14 and 15 describe interactions between counterions and protons. We assign the value 1.6 Å to r_{sh}, which is close to the O-H bond length; r_{mh} is given the value 2.7 Å (the same as r_{sm}), because the small size of a proton moving around its binding site means that we can regard it as being at the position of this site on average. Our results are insensitive to these parameters. Changing r_{sh} from 1.6 Å to 2.6 Å causes

a ~5% increase in the binding high affinity and has no effect when the counterion concentration is >0.1 nM. The effect of changing r_{mh} from 2.7 Å to 2.4 Å is even smaller. c^i_{p0} is the proton dissociation constant for a single isolated binding site (site *i*). The values of c^i_{p0} are 1.19×10^{-6} M for His, 4.83×10^{-4} M for Glu, and 1.33×10^{-3} M for Asp and other groups. These values are chosen so that we correctly obtain the experimental pK_d values of the amino acids (Lide, 2000) which have two binding sites: 6.04 for His, 4.15 for Glu, and 3.71 for Asp.

In addition, we define a long-range screening factor:

$$D(r)=1 \quad \text{for } r \le r_b \quad \text{and} \quad \exp[-\kappa(r-r_b)] \quad \text{for } r > r_b, \tag{2}$$

where κ is the Debye-Hückel screening constant, determined by the salt concentration and the pH value. If r_b is not too small, its value affects the results only slightly. The G-actin affinity data for r_b equal to 20 Å and 30 Å almost coincide if the divalent counterion concentration is <100 mM, the concentration range generally used in bundling experiments. We take r_b = 20 Å for our calculations. In our model, the bound counterions are distributed around the binding sites and their screening interactions are explicitly taken into account. The ions farther from the binding sites produce a much weaker screening. The $D(r)$ term treats this weak long-range screening in the traditional Debye-Hückel method; it is cut off at shorter distances to avoid double-counting the screening. We take the cations to be divalent and the corresponding anions to be monovalent. At high salt concentrations, the calculated screening length ($1/\kappa$) can be close to 1 Å, which is not physical. We thus set $1/\kappa$ = 10 Å when the screening length is <10 Å. Changing this cutoff to 15 Å makes no noticeable difference to our results unless the counterion concentration is very high. At 100 mM, the effect on the number of bound counterions is only 2%.

To obtain the minimum energy configuration, we let

$$\frac{\partial G_{MP}}{\partial m_i}=0 \quad \text{for sites with } q_i < 0, \tag{3}$$

and

$$\frac{\partial G_{MP}}{\partial h_i}=0 \quad \text{for sites with } q_i \le 0. \tag{4}$$

Thus, our equilibrium condition is

$$m_i=\frac{\exp\{-[U_iQ+h_ieQ/\varepsilon r_{mh}-kT\ln(c_m/c_0)]/kT\}}{1+\exp\{-[U_iQ+h_ieQ/\varepsilon r_{mh}-kT\ln(c_m/c_0)]/kT\}} \tag{5}$$

$$h_i=\frac{\exp\{-[U_ie+m_iQe/\varepsilon r_{mh}-kT\ln(c_p/c^i_{p0})]/kT\}}{1+\exp\{-[U_ie+m_ieQ/\varepsilon r_{mh}-kT\ln(c_p/c^i_{p0})]/kT\}}, \tag{6}$$

where U_i is the electrostatic potential for the bound counterion/proton at site *i*,

$$U_i=\sum_{j\ne i}\frac{q_jD(r_{ij})}{\varepsilon r_{ij}}+\sum_{j\ne i}\frac{m_jQD(r_{ij})}{\varepsilon r_{ij}}+\sum_{j\ne i}\frac{h_jeD(r_{ij})}{\varepsilon r_{ij}}+\frac{(q_i-q_{ref})}{\varepsilon r_{sm}}. \tag{7}$$

We assume that the system is always in a state of local equilibrium. The time spent in jumping between states is ignored because of the high barriers between local equilibrium states. To obtain the equilibrium state, we solve for $\{m_i\}$ and $\{U_i\}$ self-consistently using an updating method described below. The final $\{m_i\}$ are sensitive to the initial $\{m_i\}$ and the updating methods. That is to say, there are numerous local minima. Although our strategy cannot guarantee finding the global minimum, it usually finds a lower energy than using random initial $\{m_i\}$ or other updating methods that we have tried. In addition, we will see later that the most important aspects of many local minima, such as the force-distance relation between two filaments, are similar in our results.

The update procedure is as follows: from a state with no bound counterions, we find the lowest U_i site and put a counterion on it. We then update $\{U_i\}$ according to Eq. 7 and repeat the procedure until $U_i > 0$ for all sites *i*. We use the resulting $\{m_i\}$ as the initial state and update according to the following largest-error-correction algorithm: from $\{m_i\}$ and $\{h_i\}$, we obtain $\{U_i\}$ and then from $\{U_i\}$ we obtain a new set $\{m^{new}_i\}$ and $\{h^{new}_i\}$ according to Eqs. 5 and 6. Among all these sites, find the largest error $|m^{new}_k - m_k|$ (if there are two equal ones, we choose one randomly) and replace m_k with m^{new}_k. Do the same to h_k and h^{new}_k. We repeat this procedure until the largest errors are $<10^{-6}$. This largest-error-correction algorithm spontaneously breaks the symmetry of the two filaments and always finds a lower minimum than if all the $\{m_i\}/\{h_i\}$ are replaced at once. For two parallel filaments, if the environments of two sites, one on each filament, are the same, the latter algorithm assigns equal binding probabilities to the two sites; in contrast, our largest-error-correction algorithm often obtains symmetry breaking and a correspondingly lower energy.

Binding affinity hierarchy of G-actin

In addition to the work described here for actin, we have used this model to calculate the binding patterns of 14 Ca^{2+}-binding proteins in solution and correctly predict ~80% of all binding sites. The results will appear in a separate article. Here we focus on the Ca^{2+}-binding sites in actin. From the 1ATN PDB file (Kabsch et al., 1990), the structure of the complex of G-actin + ATP can be obtained by deleting chain **D** and other hetero molecules. We choose this structure because it is a suitable building block for an F-actin filament structure (Holmes et al., 1990). There are 181 sites that can bind counterions or protons, or are positively charged. In the calculations, the pH value is fixed at 7.6, which is the experimental condition in the work of Strzelecka-Golaszewska et al. (1978), and the metal ion concentration is adjusted so

that the sum of the binding probabilities of all binding sites N_{ion} is very close to N_{exp}, where N_{exp} is the number of bound ions in the PDB files. There is only one high affinity site for the G-actin+ATP complex in the PDB file, so in this case $N_{exp} = 1$. To obtain $N_{ion} = 1$, we adjust the divalent counterion concentration to 0.2 μM. The calculated binding probability at the site HETATM 4990 O2G ATP is 0.944, whereas the three negatively charged sites in the PDB file closest to the observed position of the bound ion are 2.50 Å for HETATM 4990 O2G ATP, 2.62 Å for HETATM 4993 O1B ATP, and 4.29 Å for HETATM 4991 O3G ATP. Thus the model obtains the high affinity site very precisely.

Actin will bind more counterions with increasing counterion concentration. Very weak binding cannot be detected by experiment, so we consider only $c_m < 0.1$ M. The results for N_{ion} are shown in Fig. 1 (*solid line*). The dot-dashed and dashed curves are fits of our data using simplified two- and three-level models. The better fit of the three-level model is consistent with the experimental data (Sheterline et al., 1998). The three levels are: 1), a high affinity level containing one site; 2), an intermediate affinity level containing four sites; and 3), a low affinity level containing five sites. The difference between the high affinity site and other sites is large enough that we can clearly see a shelf in the solid line. The dissociation constants fitted by three affinity levels fit the experimental values (Sheterline et al., 1998) well, as Table 1 shows.

During polymerization to form F-actin, and F-actin bundling, we find that the location of the high affinity site does not change (Fig. 2 *a*). However, polymerization dramatically changes the rest of the binding pattern. The binding pattern change induced by bundling is much smaller so that the averaged binding patterns over different monomers for the free and bundled filaments are very close. The detailed binding patterns for the free and bundled filaments (Fig. 2 *b*) show that some of the positions of the intermediate and low affinity sites differ between the free filament and the bundled filaments. These changes result from the correlations of the

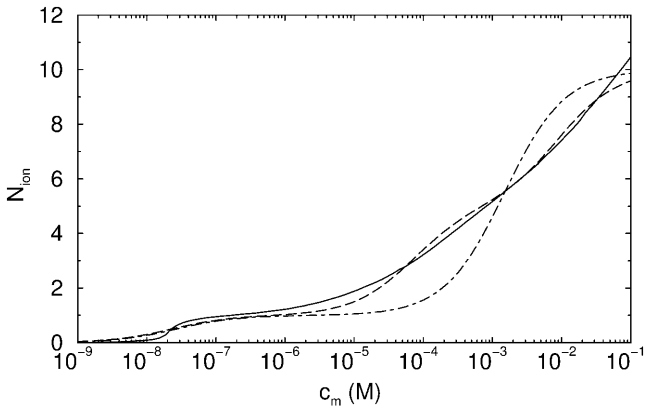

FIGURE 1 Hierarchy of binding affinities of divalent counterions to G-actin at pH = 7.6. N_{ion} is number of bound counterions; c_m is divalent counterion concentration. (*Solid line*) Numerical results; (*dot-dashed line*) two-level fit of numerical results; and (*dashed line*) three-level fit of numerical results.

TABLE 1 Comparison of three-level affinities of the counterion binding model and experiment data (Sheterline et al., 1998)

Affinity	Stoichiometry	k_d (Model)	k_d (Experiments)
High	1	23 nM	(4–40 nM), 5 nM
Intermediate	4	0.07 mM	(0.02–1.6 mM), 0.15 mM
Low	5	9 mM	(5–41 mM), 10 mM

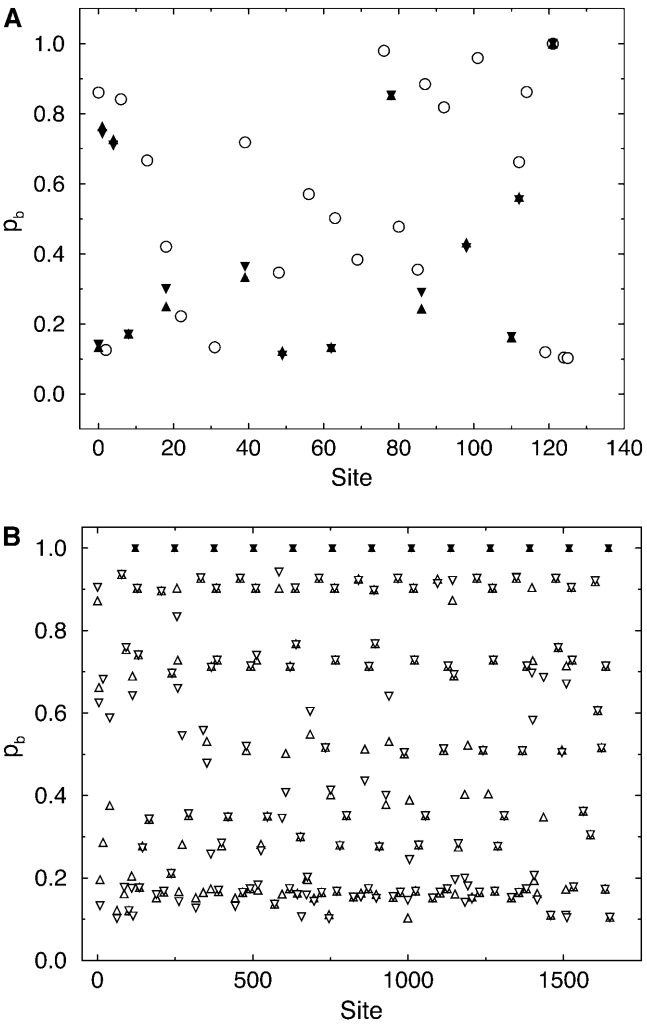

FIGURE 2 Binding patterns of G-actin, and free and bundled filaments. p_b: binding probability of a site. (*Unfilled circles*) G-actin; (*up triangles*) free filament; and (*down triangles*) bundled filament. Sites with low binding probability (<0.1) are ignored. Both filaments are in the configuration (216°, 144°, and 10.92 Å). Free filaments have separation $R = 500$ Å and bundled filaments have $R = 75.3$ Å. (*A*) Binding pattern of G-actin and averaged binding patterns of free filament and bundled filament. Different subunits in the same filament have different binding patterns, and the averaging is over one repeat unit (13 subunits). The site number of the high affinity site is 121, where all three have $p_b = 1$. (*B*) Comparison of binding patterns of free and bundled filaments in one repeat unit. Each subunit has 127 binding sites for protons and counterions. High-affinity sites are indicated by solid symbols.

counterion binding patterns in the filaments. In Fig. 2 *b*, most binding sites with $p_b > 0.8$ (including the 13 high affinity sites) have no observable change in p_b; four of them have a slight change (<0.07); and only one of them has a large change (0.2). The weak binding sites are more vulnerable to the correlations and thus their binding probabilities change more.

INTERACTION BETWEEN TWO F-ACTIN FILAMENTS

We study only the interaction between two parallel filaments. The F-actin structure is built from the 1ATN PDB file as in the work of Holmes et al. (1990). The pH is fixed at 7.2, the condition used in Tang and Janmey (1996). In the filament construction, we let the filament center line be the *z*-axis, and the bottom monomer be located at the origin. After filament *a* is built, it is rotated by an angle ϕ_a around the *z*-axis. Filament *b* is rotated by an angle ϕ_b around the *z*-axis, displaced by d_z along the *z*-axis, and moved by *R* along the *x*-axis. Thus three parameters (ϕ_a, ϕ_b, and d_z) determine a configuration of two parallel filaments. For each configuration, the center-to-center distance between the two filaments, namely *R*, is variable, and we can study the *R*-dependence of the interaction for varying configurations. F-actin is periodic with period 13 G-actins, so we let this be the length of both the filaments. We have also treated other filament lengths and find that the bundling energy is linear in the length. The angles ϕ_a and ϕ_b range from 0° to 360°; d_z ranges from 0 to $H_m/2$, where H_m is the height of a monomer in the filament (27.1 Å). We determine the minimal distance between two parallel filaments by assuming that the shortest allowed interatomic contact between the two different filaments r_{ex} is 5 Å, because there can be one counterion between them. We choose this value because for most bound divalent counterions, the distance between the counterion and its binding site is ~2.5 Å. The distance could be shorter, but our calculations show that if *R* is less than the contact distance derived from the 5 Å exclusion distance, the attractive force can rapidly change to be repulsive. This occurs because a charged site s_b in filament *b* can be closer to the center line of filament *a* than a charged site s_a in filament *a*, and the attractive force between the two sites causes the filaments repel each other. In addition, the variation of the bundling energy with r_{ex} is only ~0.01–0.02 eV/Å for the 13-monomer long filament, or 5–10% of the maximum value, and this does not affect our subsequent results strongly. In our calculations, we use a uniformly spaced mesh of 10 ϕ_a and 10 ϕ_b values: 0°, 36°, 72°, . . . , 324°. For d_z, we use 11 values: 0, 0.05 H_m, 0.10 H_m, . . . , 0.50 H_m. Thus, 1100 configurations need to be treated. All atoms are used to determine the minimal distance instead of only the charged sites and binding sites. The minimal center-to-center distances, R_c, of these configurations range from 74.5 Å to 102.1 Å, and the arithmetic average is 87.8 Å. Since configurations with shorter distances may have more contacts and thus lower energy, the thermally weighted average is much closer to 74.5 Å. This average depends somewhat on filament length; the value for 13-monomer filaments is near 75 Å, and we use this value in the simplified bundling calculations described below.

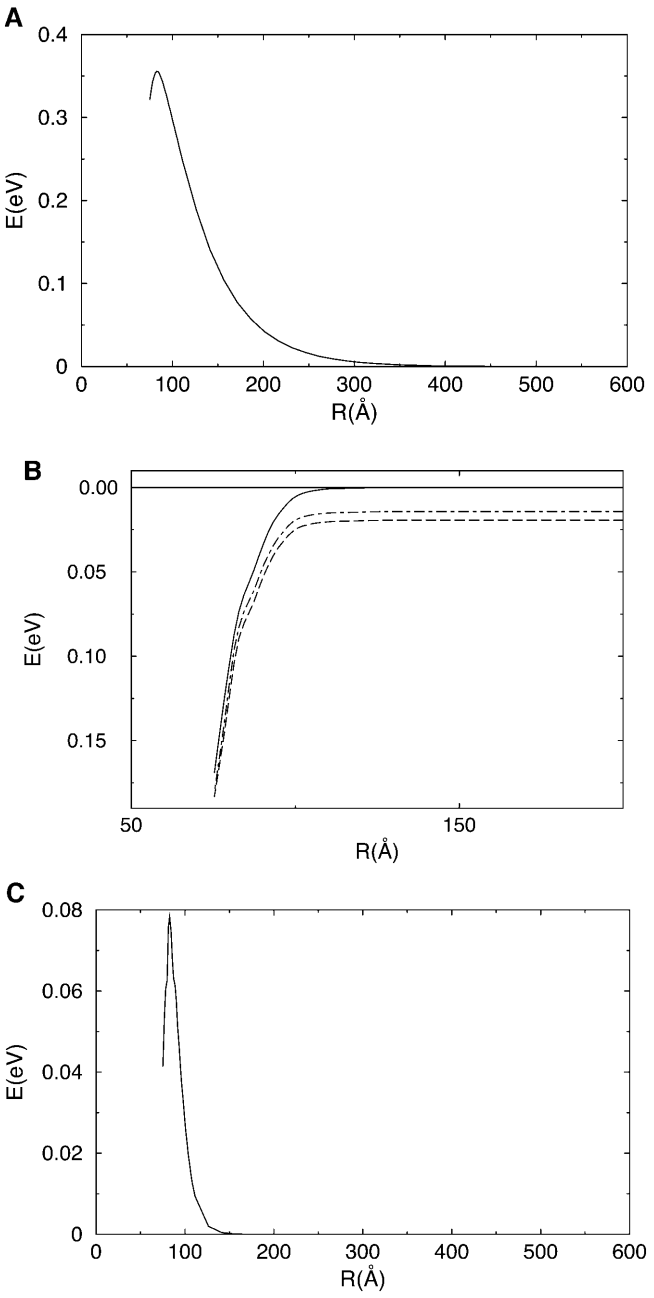

FIGURE 3 Interaction free energy *E* vs. center-to-center distance *R* between two parallel 13-subunit filaments in the two-filament configuration (216°, 144°, and 10.92 Å) at pH = 7.2 and three different divalent metal ion concentrations. (*A*) Low concentration 1 mM. (*B*) Optimal concentration 32 mM. Three different energy minima are obtained from various initial states: $R = 75.3$ Å for solid line, $R = 90.3$ Å for dot-dashed line, and $R = 87.3$ Å for dashed line. (*C*) High concentration 1.024 M.

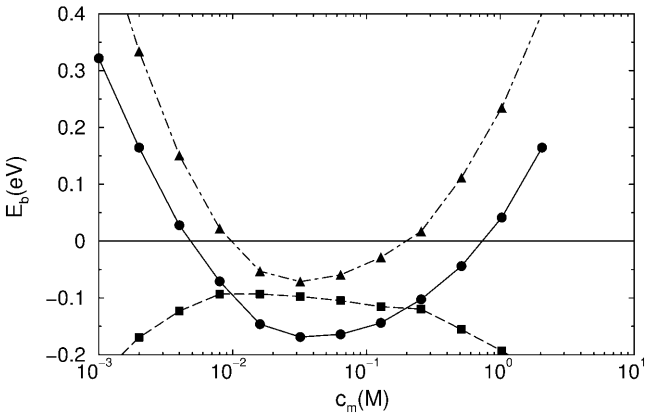

FIGURE 4 Dependences of bundling energy E_b (*circles*) for two parallel 13-subunit filaments, fixed-binding-pattern bundling energy E_b^{fix} (*triangles*), and correlation bundling energy E_b^{corr} (*squares*), on counterion concentration c_m. Lines drawn to guide the eye.

The results for three different counterion concentrations using the configuration (216°, 144°, and 10.92 Å), which gives a near-optimal bundling energy, are presented in Fig. 3, *a–c*. To optimize our solution for $\{m_i\}$, the calculations are carried out from R_c to 500 Å, and then go back to R_c. Different step sizes are used: 1.5 Å for distances <110 Å, and 15 Å for greater distances. Except the first point, each step begins with the calculated binding patterns of counterions and protons of the previous step as the initial binding probability set, and then continues with the largest-error-correction algorithm. In most cases, the returning (from far to near) curves are almost identical to the leaving curves. If not, the returning curves have a free energy slightly lower than that of the leaving curves, and are smooth. That is to say, if there is a jump between different minima, it always happens in the leaving curve. So the returning curves are regarded as the results. At low divalent counterion concentrations (Fig. 3 *a*), the two filaments are both highly negatively charged. Although there is a short-ranged attractive component, it is overwhelmed by the strong repulsive force. A long tail results from the weak screening ($1/\kappa = 55.6$ Å). At the optimal divalent counterion concentration (Fig. 3 *b*), the two filaments are almost neutralized or weakly charged. The short-ranged attraction therefore exceeds the repulsive electrostatic forces. The three different energy minima result from three different initial separations. Their force-distance behaviors are almost the same, and the bundling energies are close: −0.168 eV for the solid line, −0.166 eV for the dot-dashed line, and −0.164 eV for the dashed line. The reason for the similarity of the curves can be understood via the following simple example: there is a negatively charged site in each of the two filaments, and they are at opposing positions. Their intrafilament electrostatic environments can be different. When the filaments are close, the equilibrium states are defined by a counterion being bound at one of these two sites. Which site it is bound at does not affect the force very much, but since the intrafilament interactions may be different, the total energies may be different. Since we assume that the system is always in one of these minima, the average behavior can be represented by that of any one of the minima. Thus the problem of the global energy minimum is separate from that of the force-distance curve. At high divalent counterion concentrations (Fig. 3 *c*), the two filaments are both overcharged by counterions and thus have positive net charge. As for low concentrations, the repulsive force dominates. The screening of the salt solution is strong, leading to a rapid dropoff of the interactions.

The free energy difference between the minimal contact distance and the long-distance limit (500 Å) determines the extent of bundling, so it is called the bundling energy E_b. Our calculated value of E_b per monomer is ~0.01 eV in optimal counterion concentrations. The relation between E_b and the counterion concentration for the same configuration as in Fig. 3 is shown in Fig. 4. It is seen that there is a concentration range of a factor of ~100 for bundling. When other higher-energy configurations are included by thermal averaging, the average starting concentration for bundling is ~10 mM, close to the experimental ones. In the work of Tang and Janmey (1996), the starting concentration for Ca^{2+} is measured to be 15 mM, and that for Mg^{2+} is 25 mM. These differences may be caused by the different c_0 values of those divalent counterions.

The positive bundling energy at high divalent counterion concentrations leads to debundling. Recent experiments (Tang et al., 2002) have demonstrated this phenomenon, which is called resolubilization. In these experiments, the bundling transition is sharper than the debundling transition when plotted on linear concentration scale. In Fig. 4, E_b vs. c_m is almost symmetric around the optimal concentration on the logarithmic scale, so the calculated bundling transition would also be much sharper on a linear scale. The resolubilization happens at ~300–500 mM in our model. In the experiments (Tang et al., 2002), the debundling concentration of the ''fd'' virus is near 380 mM, and that for the M13 virus is ~220 mM. Our range of values for F-actin is close to these values.

Because previous work in the field has focused on the contribution of counterion correlation effects on bundling, we separate out the contribution of these correlations to E_b. We define E_b^{fix} (*triangles* in Fig. 4) as the bundling energy at the minimal contact distance with the binding pattern fixed to be that for the largest distance. The counterion correlation energy due to the change of the binding pattern is then $E_b^{corr} = E_b - E_b^{fix}$, which is shown as the squares. We see that E_b^{fix} is also an important part of the attractive E_b near the optimal concentration, accounting for approximately one-half of E_b. This implies that even with the counterion positions frozen, there is a substantial attractive interaction. This has been ignored in all previous work on poly-electrolyte bundling. It shows that the correlation of single-filament configurations plays an important role in bundling. E_b^{fix} is strongly

correlated with E_b. Sampling 220 of the total 1100 two-filament configurations (sampling all of them would have been computationally unwieldy) at 32 mM (the optimal concentration for most two-filament configurations), we obtain the correlation shown in Fig. 5. The difference between the best and worst two-filament configurations is close to 0.2 eV. There are even a few two-filament configurations with positive E_b at the optimal concentration. Statistically averaging using $\exp(-E_b/kT)$ as the weight shows that the few lowest energy two-filament configurations dominate the thermodynamics of the two filaments. Thus, although the two filaments are not fixed in a two-filament configuration, the correlation of configurations is crucial for bundling. This filament configuration correlation is especially important at low temperature or for longer filaments, which have a large E_b difference between the preferred two-filament configurations and others. The strong filament configuration correlation could lead to different bundling states of F-actin.

In Fig. 6, the dependence of E_b on temperature is evaluated, assuming that the model parameters are constant in a limited temperature range from 270 K to 330 K. It is seen that lower temperature gives rise to a lower divalent counterion concentration for bundling. This occurs because low temperature enhances binding of counterions, rendering the filaments closer to being charge-neutral at low divalent counterion concentrations. Assuming a minimal value $E_b = -0.1$ eV per repeat unit $= -0.008$ eV/monomer for bundling (this requirement gives reasonable values of the critical filament length for bundling in next section), the required counterion concentrations are 6.7 mM at 270 K, 10.5 mM at 300 K, and 15.7 mM at 330 K. In other words, lower temperature increases the attractive force if the counterion concentration is somewhat lower than the optimal one for the higher temperature. For example, at $c_m = 10$ mM, the values of E_b are -0.042 eV for 330 K, -0.096 eV for 300 K, and -0.133 eV for 270 K. Low temperature also lowers the counterion concentration for debundling but to a lesser extent. In this range, the temperature has no apparent effect on the value of E_b at the optimal concentration.

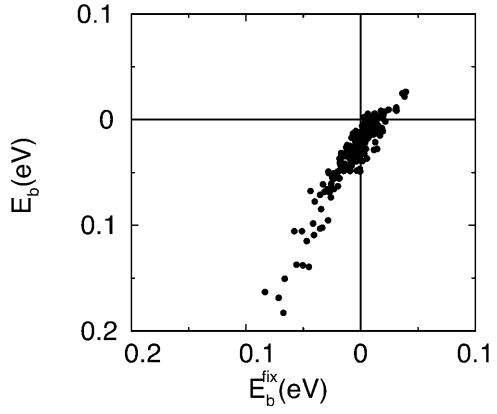

FIGURE 5 Correlation between E_b and E_b^{fix} for 220 two-filament configurations at counterion concentration of 32 mM.

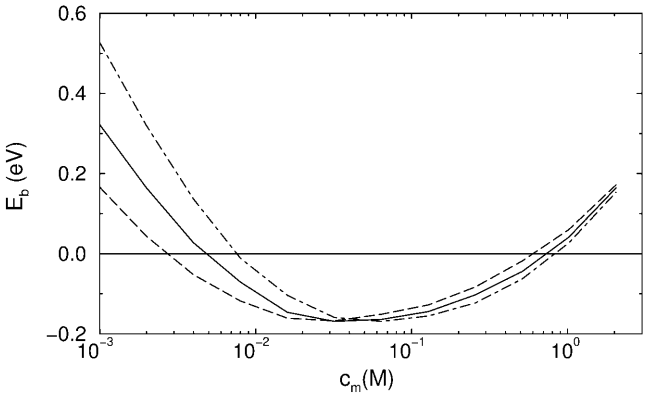

FIGURE 6 Dependence of E_b on temperature and counterion concentration for the two-filament configuration (216°, 144°, and 10.92 Å). (*Solid line*) 300 K; (*dashed line*) 270 K; and (*dot-dashed line*) 330 K.

Increasing the counterion valence decreases the c_0 value and is expected to lower the counterion concentration required for bundling. In fact, the required concentration is lowered even if we make the crude assumption that c_0 is constant (Table 2). Since the c_0 value should be larger for monovalent counterions, their optimal concentration is >1 M. Our model does not rule out the possibility that monovalent counterions can induce F-actin bundling, but the counterion concentration required is much higher than those for multivalent counterions. Experiments (Bruno and Mattice, 1992; Sedlak and Amis, 1992; Borsali et al., 1998; Manning, 2003) have shown that monovalent counterions can cause aggregation of DNA or other polyelectrolyte molecules in the dilute polyelectrolyte concentration range (we ignore the experimental reports for concentrated DNA solutions because the filament concentration is also a important factor for bundling/aggregation). To our knowledge, there are no such reports for F-actin. Experiments treating monovalent counterion concentrations up to 1 M have found no bundling (Tang, 2003, private communication).

Surprisingly, the optimal E_b does not depend strongly on the counterion valence. Although a single higher-valence counterion can mediate a stronger attractive force than a single lower-valence counterion, the number of these counterions bound to the filament is smaller. This tradeoff keeps the optimal E_b roughly constant. Because there are

TABLE 2 Effects of counterion valence on the optimal concentration c_m^{opt} and the corresponding E_b for the configuration (216°, 144°, and 10.92 Å) under the assumption of keeping c_0 constant; E_b is given for 13-monomer filaments

Valence	c_m^{opt} (M)	E_b (eV)
1	1.02	−0.166
2	0.032	−0.169
3	0.0064	−0.167

numerous positively charged sites (Arg or Lys residues) on the surface of F-actin, we find that even hypothetical counterions of valence 0.5 (which equals the magnitude of the charge of most of the negatively charged sites of F-actin in our model and cannot change the sign of these sites) can induce an attractive force of the same magnitude as that from multivalent counterions, for some two-filament configurations, and extremely high counterion concentrations. In this case, the filament configuration correlation plays a more obvious role, and the attractive force results from the interactions between the positively charged residues in one filament and the unneutralized negatively charged sites in the other filament. The role of the counterions is to reduce the repulsion between the negatively charged sites in the two filaments by neutralizing some of them.

Statistical mechanics of F-actin bundling at the two-filament level

Simplification of two-filament potential

To perform filament-bundling calculations in a computationally tractable way, we simplify the two-filament potential at the optimal counterion concentration in three steps. First, we approximate the interfilament potential of two parallel filaments by an exponential function. The energy at a center-to-center distance R of two filaments ($R > R_c$) is assumed to be

$$E(R)=E_b \exp[-(R-R_c)/R_0], \tag{8}$$

where E_b is the bundling energy at the contact distance R_c = 75 Å, and R_0 is a decay length. For all sampled configurations, the exponential function fits well with an error <0.001 eV. Second, we thermally average E_b and R_0 over different configurations. Because E_b substantially exceeds kT at the optimal counterion concentration, we are still dealing mainly with several lowest-energy configurations. Our average over the samples from the 1100 two-filament configurations gives $E_b = -0.137$ eV and $R_0 = 7$ Å. Other values are also used in calculations described below, as a sensitivity check. The third approximation is that we write $E(R)$ as a sum of effective radial monomer-monomer interactions,

$$E(R)=\sum_{i\in a, j\in b} E_{mm} \exp[-(R_{ij}-R_c)/R_1], \tag{9}$$

where a and b are two filaments containing monomers i and j respectively, R_{ij} is the distance between the centers of i and j, and R_1 is a decay length. We let the monomer-monomer interaction be zero for $R_{ij} > 100$ Å in Eq. 9. This implies that the bundling energy for parallel filaments varies fairly linearly with filament length, consistent with our results. Choosing $R_1 = R_0$ and adjusting only E_{mm}, this method gives an excellent fit for parallel orientations, with the largest error <0.001 eV for all of the E_b and R_0 values that we have tried. For skew orientations, the equation above should describe the interaction qualitatively. The statistical weight of skew orientations, in which the filaments only have a small amount of contact, is much less than those of parallel orientations (in which two filaments have a perfect contact) and free states (which contribute a much larger entropy). Thus we believe that our simplified potential can accurately describe the thermodynamics of the F-actin filaments at the optimal counterion concentration.

Two-filament bundling

To evaluate the statistical mechanics of the filament-filament interaction, we consider two filaments in a cylinder. Filament a is fixed at the center along the z-axis. The volume v_0 of the cylinder is determined by the condition that if the center of filament b is out of the cylinder, it will not interact with filament a.

In two-dimensional R–z space, where R is the center-to-center distance, the statistical weight of a point (R, z) is

$$P(R,z)=\int \exp\left(\frac{-E(R,z,\theta,\phi)}{kT}\right)\sin\theta\, d\theta\, d\phi, \tag{10}$$

where (θ, ϕ) is the orientation of filament b. The integration is restricted to the region where two filaments do not collide with each other, i.e., $E(R, z, \theta, \phi) = +\infty$ if a collision happens in this orientation of filament b. The energy of the point (R, z) is averaged over all orientations of filament b,

$$E(R,z)=\frac{\int E(R,z,\theta,\phi)\exp\left(\frac{-E(R,z,\theta,\phi)}{kT}\right)\sin\theta\, d\theta\, d\phi}{P(R,z)}. \tag{11}$$

The total statistical weight of the cylinder volume is

$$w_0=\int P(R,z)2\pi R\, dR\, dz, \tag{12}$$

and the average energy is

$$E_0=\frac{\int E(R,z)P(R,z)2\pi R\, dR\, dz}{w_0}. \tag{13}$$

We define the bundling extent of a particular position and orientation described by (R, z, θ, ϕ) as $E(R, z, \theta, \phi)/E_{min}$, where $E(R, z, \theta, \phi)$ is the energy of this position-orientation state and E_{min} is the lowest energy for all two-filament position-orientation states, which is obtained when two filaments have a complete contact. Then we take the average bundling probability for filament b restricted to v_0 to be

$$p_{b0}=\frac{E_0}{E_{min}}. \tag{14}$$

For a sufficiently low monomer concentration (the filament concentration is measured by the corresponding

monomer concentration), two filaments will typically occupy a volume $v > v_0$, and one readily shows that

$$p_b = \frac{p_{b0} w_0}{w_0 + 4\pi(v - v_0)}, \quad (15)$$

where 4π is the orientational statistical weight of a point outside of v_0 where filament b can rotate freely without contacting filament a. The complete calculation for a two-filament system of a certain length consists of two steps: integration over the orientation space of filament b (Eq. 11), and integration over its R–z coordinates (Eq. 13). The orientation and R–z coordinate spaces are divided into small cells, and a point in each cell is randomly chosen to represent the cell because this allows us to check the accuracy of the calculations conveniently. The cells are chosen small enough so that two calculations with different point sets have nearly identical results. In general, the resulting difference between two p_{b0} values is <0.5%.

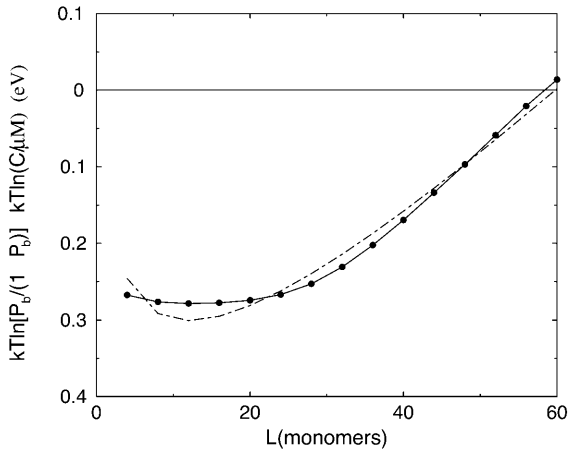

FIGURE 7 Dependence of bundling probability on filament length and subunit concentration. Significance of vertical axis is discussed in text. (*Solid line*) Numerical results at subunit concentration $C = 1\ \mu$M. Numerical results at $C = 2\ \mu$M are indistinguishable from 1 μM results. (*Dot-dashed line*) Fit of numerical results according to Eq. 19, as $kT\ln(p_b/1 - p_b) - kT\ln(C/C_0) = 0.0106\,\text{eV} \times L - 0.112\,\text{eV} - 0.127\,\text{eV} \times \ln(L)$.

RESULTS

Using our averaged E_b and R_0 values (−0.137 eV and 7 Å), we can obtain the critical bundling length L_c, which is defined as the filament length L required for $p_b = 1/2$ at a certain monomer concentration. To evaluate the sensitivity of our results to variations in the values of E_b and R_0, we present in Table 3 results for eight $\{E_b, R_0\}$ pairs at a monomer concentration of 1 μM, chosen to test the effects of 20–30% variations in the parameters. In cases having L_c >90 Å, the results are obtained by using a linear fit as discussed below. Lower E_b values and larger R_0 values enhance bundle formation and shorten L_c. L_c is more sensitive to E_b than to R_0, because E_b determines the statistical weight of the bundled state exponentially and R_0 only affects it linearly. In the range of $-0.15\ \text{eV} \le E_b \le -0.10\ \text{eV}$ and $5\ \text{Å} \le R_0 \le 7\ \text{Å}$, L_c is between 50 and 100 monomers. The dependence of p_b at 1 μM on L for {−0.137 eV, 7 Å} is shown in Fig. 7. The form of the function on the y-axis is explained below; $y = 0$ is the cutoff value for bundling. When the actin concentration is 1 μM, L_c is 59 monomers. Increasing the actin concentration does not reduce L_c much. For instance, L_c is 54 monomers at concentration of 7 μM. The experimental value (Tang and Janmey, 1996) is ~50 monomers at the same pH value (7.2) and an actin concentration of 4.6 μM (0.2 mg/ml), using a different bundling agent (Lys_{18} with a high valence). The approximate independence of the optimal E_b from the counterion valence (Table 2) means that we can legitimately compare our results to this experimental value.

TABLE 3 Critical bundling lengths for different E_b and R_0 values at monomer concentration of 1 μM

E_b (eV)	−0.090	−0.100	−0.137	−0.150
$R_0 = 5$ Å	116	101	73	65
$R_0 = 7$ Å	94	82	59	52

To explain the bundling behavior shown in Fig. 7, we solve a simple two-state model. In this model, the two-filament system has two states: bundled and free, with free energies F^b and F^f, respectively. The monomer concentration C affects only the entropy of the free state. The average volume v occupied by the two filaments is determined by C and L. Most of this volume belongs to the free state. Therefore,

$$F^f = F_0^f + kT\ln(C/C_0) - kT\ln(L/L_0), \quad (16)$$

where C_0 is a reference concentration, taken to be 1 μM; L_0 is a reference filament length; and F_0^f is the free energy for L_0 and C_0. Neither C_0 nor L_0 affects the final results, but we give a value for C_0 to avoid taking the logarithm of a nondimensionless quantity. The enthalpy of the bundled state is proportional to L. L affects the entropy of the bundled state relative to that of the free state in two ways. First, because of steric hindrance, the longer the filaments, the more restricted are the orientations of the bundled filament b. Second, at a fixed monomer concentration C, the volume for the free state increases as L increases, but the volume for the bundled state does not change much, because its main contribution to the partition function comes from a narrow region in translational phase space where the center of filament b is close to that of filament a (especially for the long filaments). These factors appear in the free energy at most in the order of $\ln(L)$. Thus, the free energy difference can be written as

$$F^{b} - F^{f} = -kT\ln(C/C_0) - a_1 L - a_0 + a_2\ln(L), \quad (17)$$

where the first term is the negative of the translational entropy in the free state, the second term is the filament binding energy, and the remaining terms account for the loss in rotational entropy, and corrections to the translational entropy. a_1 is expected to be positive since the bundling energy is negative, and a_2 should also be positive since the angular freedom of the bundled state decreases and the volume of the free state increases with increasing L. In addition,

$$\frac{p_b}{1-p_b} = \exp[-(F^{b} - F^{f})/kT]. \quad (18)$$

Therefore,

$$kT\ln\left(\frac{p_b}{1-p_b}\right) - kT\ln(C/C_0) = a_1 L + a_0 - a_2\ln(L). \quad (19)$$

This equation gives a satisfactory fit (*dot-dashed line*) to the computational data (*solid line*) as shown in Fig. 7. The 2 μM results that we obtain are essentially indistinguishable from the 1-μM results. This confirms that the contribution from C is mainly included in the term $kT\ln(C/C_0)$, as is assumed in Eq. 17. For small L, the energy reduction from increasing L cannot compensate for the loss in entropy in the bundled state, and p_b slopes down. With further increasing L, the magnitude of the bundling energy increases proportionally to L, and dominates the entropy loss, which is at most proportional to $\ln(L)$.

To obtain a better fit for extrapolating to larger L values, we develop a further approximation. In a narrow region of large L, we can assume that the entropy loss is nearly constant, so that

$$kT\ln\left(\frac{p_b}{1-p_b}\right) - kT\ln(C/C_0) = \alpha L + \beta. \quad (20)$$

We use this equation to fit the four points of length from 48 to 60 monomers and obtain $\alpha = 0.0093$ eV/monomer, $\beta = -0.54$ eV. The value of α is close to minus the energy change resulting from adding a monomer to each filament in the closest contact two-filament configuration, which is 0.0105 eV/monomer.

Our two-filament model is only an approximation, and it works when multifilament cooperative effects are not strong. The multifilament interactions are not additive, as discussed in Ha and Liu (1999) and Podgornik and Parsegian (1998), due to competition between the binding pattern correlations and/or the configuration correlations. We note that Sear also studied the bundling resulting from the interaction between two filaments using an analytic model (Sear, 1997). We estimate the critical bundling length for $E_b = -0.01$ eV/monomer and $R_0 = 7$ Å from his Eq. 4, and obtain 80 monomers. This is close to our exact result of 59 monomers.

CONCLUSIONS

We have analyzed an Ising-like counterion binding model which accurately describes the binding of divalent counterions to proteins. This model confirms the three affinity levels for divalent counterion binding sites of G-actin, with the correct binding affinities. By solving the model for two F-actin filaments, we have obtained the bundling interaction. During polymerization and bundling, the high-affinity site is unaffected but others are substantially repopulated. The difference in binding pattern induced by bundling is much smaller than that caused by polymerization. The attractive force results not only from the binding pattern correlations but from the filament configuration correlations with fixed binding patterns as well. The bundling energy depends strongly on the configuration of the filaments. The results show that a divalent counterion concentration between 10 mM and 300 mM is needed to produce a sufficient attraction for F-actin bundling. Too high a divalent counterion concentration results in debundling. At the optimal counterion concentration, the bundling energy per monomer along the filament for near-optimal configurations is ~ -0.01 eV. Although the valence of the counterions strongly affects the optimal counterion concentration, it does not strongly affect the optimal-concentration bundling energy. Finally, simplifying the bundling interaction to a sum of monomer-monomer interactions has allowed us to study the statistical mechanics of F-actin bundling. We obtain a critical bundling length that is close to the experimental value.

We are grateful to Prof. David Sept, Prof. Jay Tang, and Silvina Zapata for informative conversations. We also thank the Referees for helpful comments.

The work was supported by the National Institutes of Health under grant GM38542.

REFERENCES

Baeza, I., P. Garislio, L. M. Rangel, P. Chavez, L. Cervants, C. Arguello, C. Wong, and C. Montanez. 1987. Electron microscopy and biochemical properties of polyamines-compacted DNA. *Biochemistry*. 26:6387–6392.

Bednar, J., P. Furrer, A. Stasiak, J. Dubochet, E. H. Egelman, and A. D. Bates. 1994. The twist, writhe and overall shape of supercoiled DNA change during counterion-induced transition from a loosely to a tightly interwound superhelix. *J. Mol. Biol.* 235:825–847.

Bloomfield, V. A. 1996. DNA condensation by multivalent cations. *Curr. Opin. Struct. Biol.* 6:334–341.

Bloomfield, V. A. 1997. Polyelectrolyte effects in DNA condensation by polyamines. *Biophys. Chem.* 11:339–343.

Borsali, R., H. Nguyen, and R. Pecora. 1998. Small-angle neutron scattering and dynamic light scattering from a polyelectrolyte solution: DNA. *Macromolecules*. 31:1548–1555.

Borukhov, I., K.-C. Lee, W. M. Gelbart, A. J. Liu, and M. J. Stevens. 2002. Association of two semiflexible polyelectrolytes by interchain linkers: theory and simulations. *J. Chem. Phys.* 117:462–480.

Brooks, B. R., R. E. Bruccoleri, B. D. Olafson, D. J. States, S. Swaminathan, and M. Karplus. 1983. CHARMM: a program for macromolecular energy, minimization, and dynamics calculations. *J. Comp. Chem.* 4:187–217.

Bruno, K. R., and W. L. Mattice. 1992. Long-range intermolecular interactions in dilute aqueous solutions of ionized poly(L-lysine) at low ionic strength. *Macromolecules*. 25:327–330.

Deserno, M., and C. Holm. 2002. Theory and simulations of rigid polyelectrolytes. *Mol. Phys*. 100:2941–2956.

Diehl, A., H. A. Carmona, and Y. Levin. 2001. Counterion correlations and attraction between like-charged macromolecules. *Phys. Rev. E*. 64: 011804.

Gelbart, W. M., R. F. Bruinsma, P. A. Pincus, and V. A. Parsegian. 2000. DNA-inspired electrostatics. *Phys. Today*. 53:38–44.

Grønbech-Jensen, N., R. J. Mashl, R. F. Bruinsma, and W. M. Gelbart. 1997. Counterion-induced attraction between rigid polyelectrolytes. *Phys. Rev. Lett*. 78:2477–2480.

Ha, B.-Y., and A. J. Liu. 1997. Counterion-mediated attraction between two like-charged rods. *Phys. Rev. Lett*. 79:1289–1292.

Ha, B.-Y., and A. J. Liu. 1999. Counterion-mediated, non-pairwise-additive attractions in bundles of like-charged rods. *Phys. Rev. E*. 60:803–813.

Holmes, K. C., D. Popp, W. Gebhard, and W. Kabsch. 1990. Atomic model of the actin filament. *Nature*. 347:44–49.

Kabsch, W., H. G. Mannherz, D. Suck, E. F. Pai, and K. C. Holmes. 1990. Atomic structure of the actin: DNase I complex. *Nature*. 347:37–44.

Kawamura, M., and K. Maruyama. 1970. Polymorphism of F-actin. I. Three forms of paracrystals. *J. Biochem. (Tokyo)*. 68:885–899.

Kornyshev, A. A., and S. Leikin. 1998. Electrostatic interaction between helical macromolecules in dense aggregates: an impetus for DNA poly- and meso-morphism. *Proc. Natl. Acad. Sci. USA*. 95:13579–13584.

Lau, A. W. C., and P. Pincus. 2002. Counterion condensation and fluctuation-induced attraction. *Phys. Rev. E*. 66:041501.

Lide, D. R. (Editor-in-chief.) 2000. CRC Handbook of Chemistry and Physics, 81st Ed. CRC Press, Boca Raton, Florida. **7**-1.

Ma, C., and V. A. Bloomfield. 1994. Condensation of supercoiled DNA induced by $MnCl_2$. *Biophys. J*. 67:1678–1681.

Manning, G. S. 2003. Comments on selected aspects of nucleic acid electrostatics. *Biopolymers*. 69:137–143.

Moreira, A. G., and R. R. Netz. 2001. Binding of similarly charged plates with counterions only. *Phys. Rev. Lett*. 87:078301.

Oosawa, F. 1968. Interaction between parallel rodlike macroions. *Biopolymers*. 5:1633–1647.

Podgornik, R., and V. A. Parsegian. 1998. Charge-fluctuation forces between rodlike polyelectrolytes: pairwise summability reexamined. *Phys. Rev. Lett*. 80:1560–1563.

Ray, J., and G. S. Manning. 1994. An attractive force between two rodlike polyions mediated by sharing of condensed counterions. *Langmuir*. 10:2450–2461.

Sear, R. P. 1997. Cohesion and aggregation of flexible hard rods with an attractive interaction. *Phys. Rev. E*. 55:5820–5824.

Sedlak, M., and E. J. Amis. 1992. Concentration and molecular weight regime diagram of salt-free polyelectrolyte solutions as studied by light scattering. *J. Chem. Phys*. 96:826–834.

Sheterline, P., J. Clayton, and J. C. Sparrow. 1998. Actin, 4th Ed. Oxford University Press, New York. 16.

Shklovskii, B. I. 1999. Screening of a macroion by multivalent ions: correlation-induced inversion of charge. *Phys. Rev. E*. 60:5802–5811.

Stevens, M. J. 1999. Bundle binding in polyelectrolyte solutions. *Phys. Rev. Lett*. 82:101–104.

Stevens, M. J. 2001. Simple simulations of DNA condensation. *Biophys. J*. 80:130–139.

Strzelecka-Golaszewska, H., E. Prochniewicz, and W. Drabikowski. 1978. Interaction of actin with divalent cations. II. Characterization of protein-metal complexes. *Eur. J. Biochem*. 88:229–237.

Tang, J. X., and P. A. Janmey. 1996. The polyelectrolyte nature of F-actin and the mechanism of actin bundle formation. *J. of Bio. Chem*. 271: 8556–8563.

Tang, J. X., S. Wong, P. T. Tran, and P. A. Janmey. 1996. Counterion-induced bundle formation of rodlike polyelectrolyte. *Ber. Bunsenges. Phys. Chem*. 100:796–806.

Tang, J. X., J. A. Käs, J. V. Shah, and P. A. Janmey. 2001. Counterion-induced actin ring formation. *Eur. Biophys. J*. 30:477–484.

Tang, J. X., P. A. Janmey, A. Lyubartsev, and L. Nordenskiöld. 2002. Metal ion-induced lateral aggregation of filamentous viruses. *Biophys. J*. 83:566–581.